

Continuous Wave Thin Plate Nd:Glass Laser

FERENC KRAUSZ, E. WINTNER, ARNOLD J. SCHMIDT, AND ANDREW DIENES

Abstract—We model CW operation of end-pumped four-level glass lasers to obtain expressions for threshold, slope efficiency, and figures of merit. Discussion of thermal effects ultimately limiting performance in these lasers is also given. Basic design considerations for optimum performance of an end-pumped CW Nd:glass laser intended for mode locking are presented. Based on these investigations we have built a CW Nd:glass laser containing a heavily-doped thin phosphate glass plate as the gain material. The plate was inserted into a folded cavity and pumped longitudinally by a Kr laser at $0.8 \mu\text{m}$. With 2.5 percent output coupling the pump threshold and the slope efficiency well above threshold were measured to be 10.5 mW and 36 percent, respectively. These values agree reasonably with theoretical predictions. Experimental confirmation of the predicted thermal limiting effects are also obtained.

I. INTRODUCTION

NEODYMIUM:glass lasers generating intense picosecond pulses [1], [2] have been important research tools for over two decades. The conventional broad-band flash lamp pumping of Nd:glass produces much undesirable heat by the short wavelength components. Thus, water cooling is needed and pulses can be generated only at low repetition rates ($\approx 1 \text{ Hz}$) and poor stability [3]. There is great interest in obtaining highly-stable CW trains of picosecond pulses allowing 1) fast data acquisition and 2) pulse compression down to the femtosecond regime.

To achieve sufficient gain in CW operation without thermal problems, narrow line (laser) pumping at photon energies as low as possible is desirable. A longitudinal pumping scheme is the best choice for high optical to optical efficiency [4]. The fortunate coincidence of the lowest energy pump band of Nd with the emission spectrum of high-power GaAlAs diode lasers offers the possibility of both low thermal loading and high electrical to optical efficiency [5]. Although two groups [5]–[7] have reported successful mode locking of a laser-pumped CW Nd:glass laser, no attempt has been made so far to analyze and optimize the performance of a CW Nd:glass laser suit-

able for mode locking. This is the subject of the present paper with the aim to design and build an efficient CW Nd:glass laser operating at $1.054 \mu\text{m}$ and suitable for stable ultrashort pulse generation.

To describe CW glass laser behavior properly we generalize the theory of end-pumped homogeneously-broadened solid-state lasers for the case of additional inhomogeneous broadening. Because of the high gain necessary for stable mode locking we also discuss thermal effects which ultimately limit the laser performance both in CW and in CW mode-locked operation. Our investigations allow to draw important conclusions concerning host (glass) selection, design considerations, and pump power limitation. They apply for all glass lasers irrespective of dopants. Experimental results are presented supporting the theoretical analysis and design predictions.

II. SPECTROSCOPIC PROPERTIES OF Nd^{3+} IN GLASSES

Dopant ions in glass laser media experience different perturbing local fields in a great variety of physical environments. Site-to-site differences in energy levels, transition probabilities, and orientations of the lasing ions result in a distribution of the spectroscopic properties [8]. These inhomogeneities give rise to selective depletion of subsets of the inverted population by the laser beam. The selective deexcitations of ions in laser glasses cause hole burning of two general types: spectral and polarization [9].

Obviously, such a great variety of spectroscopic inhomogeneities can be treated analytically only if some basic simplifications are made. The first step toward a simple model is to replace the actual spectroscopic parameters (lifetime, cross sections, homogeneous linewidths) of the individual ions by average numbers. The variations of these parameters from site-to-site are considered as second-order corrections and not discussed in the present work. The laser transition ${}^4F_{3/2}$ – ${}^4I_{9/2}$ consists of a number of Stark transitions, as a consequence of the Stark splitting of the upper and lower laser levels. Nevertheless, the inhomogeneous linewidth $\Delta\nu_{\text{inh}}$ in most glasses are on the order of the average difference $\Delta\nu_{\text{av}}$ between adjacent Stark-frequencies, thereby resulting in a single broad and smooth fluorescence line [10].

The magnitude of the homogeneous linewidth $\Delta\nu_h$ plays a fundamental role in the saturation behavior of neodymium laser glasses. We consider two limiting cases. In the

Manuscript received February 15, 1989; revised July 23, 1989. This work was supported in part by the Hochschuljubiläumstiftung der Gemeinde Wien and by the Fonds zur Förderung der wissenschaftlichen Forschung in Österreich under Project Number P 7282.

F. Krausz, E. Wintner, and A. J. Schmidt are with Abteilung Quantenelektronik und Lasertechnik, Technische Universität Wien, A-1040 Wien, Austria.

A. Dienes was with the Abteilung Quantenelektronik und Lasertechnik, Technische Universität Wien, A-1040 Wien, Austria, on leave from the Department of Electrical and Computer Science, University of California, Davis, CA 95616.

IEEE Log Number 8931628.

limit where $\Delta\nu_h$ is considerably smaller than $\Delta\nu_{av}$, a sharp hole is “burnt” in the fluorescence profile by a narrow line saturating beam, and the saturation is mostly influenced by the parameter $\Delta\nu_h/\Delta\nu_{inh}$. The sharp hole is accompanied by a slight decrease of the fluorescence across the whole line as a consequence of uncorrelated inhomogeneous broadening of the individual Stark transitions [11], [12]. The above relation between $\Delta\nu_h$ and $\Delta\nu_{av}$ holds, e.g., in silicate glasses, in which the Stark splitting is relatively strong. Accordingly, easily observable spectral hole burning occurs in gain saturation experiments [13].

The other limit is $\Delta\nu_h \geq \Delta\nu_{av}$. In this case it proves meaningful to introduce an effective homogeneous line (EHL) which describes the fluorescence of a subset of ions having the same Stark frequencies within the laser transition. The EHL includes all transitions from the thermally-populated Stark sublevels of the metastable level to the Stark manifold of the terminal level. The fast thermalization ($\tau_{th} \leq 1$ ps) between Stark states allows us to refer to this line as a quasi-homogeneous one. In a first approximation, we assume that spectral inhomogeneities cause the EHL of another subset of ions just to be shifted without any significant change in its shape. Again, deviations from this behavior are considered as second-order corrections and left out of account.

Under these conditions gain saturation is governed by the parameter $\Delta\nu_{ch}/\Delta\nu_{inh}$ instead of $\Delta\nu_h/\Delta\nu_{inh}$, where $\Delta\nu_{ch}$ is the width of the EHL. Consequently, there is no spectral hole burning expected because $\Delta\nu_{ch}$ is usually greater than $\Delta\nu_{inh}$. This second limiting case may be possibly reached in some phosphate glasses, in which the Stark splitting appears to be considerably weaker than in silicate glasses [14].

Polarization inhomogeneity arises from anisotropy of the stimulated emission cross section [15]. As a result, polarization hole burning occurs if the gain is saturated by a polarized beam. Nevertheless, the influence of polarization inhomogeneity on gain saturation is smaller than that of spectral inhomogeneity, and will be ignored in the following discussion.

III. MODELING CW OPERATION IN END-PUMPED Nd:GLASS LASERS

Threshold pump power and slope efficiency are the two important parameters characterizing CW laser behavior. A number of researchers have developed rate equation models for end-pumped solid-state lasers yielding expressions of the above parameters are four-level [16]–[18] and quasi-three-level lasers [19]. All of these models suppose a homogeneously-broadened laser transition. We improve these models for the general case where both homogeneous and inhomogeneous broadening is present. Polarization inhomogeneities are neglected in our model. This is especially justified if the pump beam is polarized because in this case selective excitation of an oriented subset of ions occurs.

The circulating power in a low-loss oscillator is approximately the same in both directions. Therefore, the

increase in power after one round-trip can be written

$$\Delta P = 2G_{rs}(P_{in}, P)P - \delta P \quad (1)$$

where $G_{rs}(P_{in}, P)$ is the single-pass gain depending on the input pump power P_{in} , on the circulating signal power P , and on pump and signal intensity distributions $r(x, y, z)$ and $s(x, y, z)$. δ is the round-trip cavity loss. From (1) P is related to the incident pump power under steady-state conditions:

$$G_{rs}(P_{in}, P) - \delta/2 = 0. \quad (2)$$

The output power is simply given by

$$P_{out} = TP \quad (3)$$

where T is the transmission of the output coupler. To derive the expression of $G_{rs}(P_{in}, P)$ we assume the laser transition to consist of a single line broadened both homogeneously and inhomogeneously. At the end of the calculations we apply our results for the two limiting cases $\Delta\nu_h \ll \Delta\nu_{av}$ and $\Delta\nu_h \geq \Delta\nu_{av}$ discussed in the preceding section.

The rate equations describing interaction between a narrow line radiation and a four-level system are as follows:

$$\frac{\partial I(\mathbf{r})}{\partial z} = I(\mathbf{r}) \int_0^\infty \sigma_h(\nu_l, \nu') n(\nu', \mathbf{r}) d\nu' \quad (4)$$

$$\begin{aligned} \frac{\partial n(\nu, \mathbf{r})}{\partial t} = & W(\mathbf{r}) N_0 g(\nu, \nu_0) - \frac{n(\nu, \mathbf{r})}{\tau} \\ & - n(\nu, \mathbf{r}) \sigma_h(\nu_l, \nu) \frac{I(\mathbf{r})}{h\nu_l} \end{aligned} \quad (5)$$

where $I(\mathbf{r})$ is the signal intensity, $\sigma_h(\nu, \nu')$ represents the homogeneously-broadened stimulated emission cross section of a subset of ions with central frequency ν' , and $n(\nu, \mathbf{r})$ is the number of inverted ions per unit volume per unit frequency interval. $W(\mathbf{r})$ stands for the pumping rate, N_0 is the dopant concentration, $g(\nu, \nu_0)$ is the equilibrium shape of the inhomogeneous spectral line centered at ν_0 and normalized to unity, and τ denotes the lifetime of the metastable level. N_0 is assumed to be sufficiently high so that the threshold can be reached without significant depletion of the ground-state population. Cross relaxation [20] is not included in (4) and (5) because it significantly takes place only on a time scale of $> \tau$ [21]. The pump rate $W(\mathbf{r})$ is assumed to be frequency-independent.

Actually, this is a good approximation also in the case of narrow line pumping, because accidental coincidences between different Stark transitions within the absorption line result in a nearly-equal excitation of spectrally-different subsets of ions over the entire inhomogeneously-broadened profile. We obtain the steady-state gain coefficient from (4) and (5) by setting $\partial n/\partial t = 0$:

$$\gamma(\mathbf{r}) = W(\mathbf{r}) \tau N_0 \int_0^\infty \frac{\sigma_h(\nu_l, \nu') g(\nu', \nu_0)}{1 + 2I(\mathbf{r}) \sigma_h(\nu_l, \nu') \tau / (h\nu_l)} d\nu'. \quad (6)$$

The factor 2 reflects the fact that the gain is saturated by the sum of the intensities of the counterpropagating signal waves, which is a reasonable approximation for a large number of oscillating longitudinal modes.

In the following we assume a Lorentzian homogeneous and a Gaussian inhomogeneous line. It is convenient to introduce the pump and signal distribution functions $r(x, y, z)$ and $s(x, y, z)$, normalized to unity over space and area, respectively, so that

$$W(\mathbf{r})N_0 = Rr(x, y, z) \quad (7)$$

and

$$I(\mathbf{r}) = Ps(x, y, z) \quad (8)$$

where R is the pumping rate:

$$R = \eta_a \eta_p \frac{P_{\text{in}}}{h\nu_p} \quad (9)$$

η_a is the fraction of the incident pump power absorbed in the gain medium, and η_p denotes the pumping quantum efficiency, which is the ratio of the number of ions excited to the upper laser level to the number of absorbed photons.

Making use of (6)–(9), supposing again low loss (and thus low gain), and with $\nu_l = \nu_0$, G_{rs} takes the form

$$G_{\text{rs}}(P_{\text{in}}, P) = \eta_a \eta_p \frac{\sigma_h \tau P_{\text{in}}}{h\nu_p} \cdot \int \frac{V(\beta) s(x, y, z) r(x, y, z)}{1 + (2P/I_s) s(x, y, z)} dv \quad (10)$$

where the volume integration is over that of the active medium. $V(\beta)$ represents the convolution of a Lorentzian and Gaussian distribution, the well-known Voigt integral [22]:

$$V(\beta) = \frac{1}{\beta \sqrt{\pi}} \int_{-\infty}^{+\infty} \frac{e^{-(u/\beta)^2}}{1 + u^2} du \quad (11)$$

where

$$\beta = (\ln 2)^{-1/2} \Delta\nu_{\text{inh}}/\Delta\nu_h(I). \quad (12)$$

$\Delta\nu_h(I)$ is the power-broadened homogeneous linewidth [23]:

$$\nu_h(I) = \Delta\nu_h(1 + 2I/I_s)^{1/2} \quad (13)$$

and $I_s = h\nu_l/(\sigma_h \tau)$ is the saturation intensity. σ_h denotes the maximum value of the homogeneously-broadened cross section. Combining (2) and (10) the connection between the pump power and the circulating signal power is obtained in an inhomogeneously-broadened four-level laser.

With the substitution of $P = 0$ the threshold pump power from (2) and (10) is given by

$$P_{\text{th}} = \frac{h\nu_p \delta}{2\sigma\tau} \frac{1}{\eta_a \eta_p} \frac{1}{F_0} \quad (14)$$

where

$$F_0 = \int s(x, y, z) r(x, y, z) dv \quad (15)$$

and σ is the effective emission cross section including inhomogeneous broadening. The relation between σ_h and the experimentally directly accessible σ is

$$\sigma = \sigma_h V[\beta(I = 0)]. \quad (16)$$

The other important parameter describing CW laser behavior is the slope efficiency

$$\eta_{\text{sl}} = T \frac{dP}{dP_{\text{in}}}. \quad (17)$$

From (2) it follows that

$$dG_{\text{rs}} = \frac{\partial G_{\text{rs}}}{\partial P_{\text{in}}} dP_{\text{in}} + \frac{\partial G_{\text{rs}}}{\partial P} dP = 0. \quad (18)$$

Before calculating these derivatives we replace the position-dependent $V(\beta)$ in (10) by a position-independent effective value of $V(\beta)$. Thus, we define and calculate the quantity

$$\eta_e(P) = V[\beta(I_{\text{av}})] \quad (19)$$

which may be referred to as power extraction efficiency of an inhomogeneously-broadened transition. I_{av} is the spatially-averaged signal intensity. This step allows us a clear interpretation of η_{sl} in terms of various contributions reducing the efficiency. Now, from (2), (10), (17), and (18) the slope efficiency is found after some calculations to be

$$\eta_{\text{sl}} = \frac{T h\nu_l}{\delta h\nu_p} \eta_a \eta_p \eta_e \eta_c \quad (20)$$

where η_c is the coupling efficiency

$$\eta_c = F_1^2/F_2 \quad (21)$$

with

$$F_1 = \int \frac{s(x, y, z) r(x, y, z)}{1 + (2P/I_s) s(x, y, z)} dv \quad (22)$$

and

$$F_2 = \int \frac{s^2(x, y, z) r(x, y, z)}{[1 + (2P/I_s) s(x, y, z)]^2} dv. \quad (23)$$

η_c originates from the incomplete extraction of all the excitations because of the transverse variations of intensity of both the pump beam and the laser cavity mode. Substituting $P = 0$ the expression of η_c agrees with that in [16] derived in a somewhat different way for the pumping region near threshold.

Both the power extraction efficiency and the geometrical coupling efficiency are functions of the signal power circulating in the cavity representing a nonlinear connection between input and output powers. For the description

of this dependence we introduce the normalized quantity $S = 2P/I_s \pi w_l^2$, which may be termed saturation parameter. It roughly gives the ratio of the induced and spontaneous emission powers. I_s can be expressed in terms of experimentally accessible quantities by using (16): $I_s = h\nu_l V(\beta_0)/(\sigma\tau)$, where $\beta_0 = \beta(I=0)$.

η_e is plotted as a function of $\Delta\nu_{\text{inh}}/\Delta\nu_h$ for various saturation parameters in Fig. 1. The increase of $\Delta\nu_{\text{inh}}/\Delta\nu_h$ reduces the fraction of the upper-state population which participates in stimulated emission thereby giving rise to a reduction of η_e . On the other hand, saturation causes power broadening of the homogeneous line [23], thus η_e increases with increasing S for a fixed $\Delta\nu_{\text{inh}}/\Delta\nu_h$.

In the most important practical case both $s(x, y, z)$ and $r(x, y, z)$ have a Gaussian transversal distribution. Neglecting diffraction s is independent of z , and the z -dependence of $r(x, y, z)$ accounts for the absorption of the pump light in the active medium, which is assumed to be unsaturated because of the low inversion needed to reach threshold. Assuming both the resonator mode and the pump beam to be Gaussian, the threshold from (14) and (15) is computed to be

$$P_{\text{th}} = \frac{h\nu_p \delta}{2\sigma\tau} \frac{1}{\eta_a \eta_p} \frac{\pi}{2} \overline{w_l^2} (1 + \mu). \quad (24)$$

$\mu = \overline{w_p^2}/\overline{w_l^2}$ where w_l and w_p are signal and pump spot sizes, respectively. Diffraction of pump beam and cavity mode within the gain medium is taken into account at the end of the calculations by replacing w_l^2 and w_p^2 by their averaged values $\overline{w_l^2}$ and $\overline{w_p^2}$. The averaging is carried out along the length L of the active medium. This is a reasonable approximation as long as L is not longer than the confocal parameters of both beams. Here and throughout this paper $\overline{w_l^2}$ and $\overline{w_p^2}$ are simplified notations for $w_{lx} w_{ly}$ and $w_{px} w_{py}$, respectively [24].

Not surprisingly, (24) has the same form for inhomogeneous as for homogeneous broadening with the only difference in the reduced magnitude of σ due to inhomogeneous broadening. This similarity clearly reflects the fact that differences between the behaviors of the two systems appear only when they get saturated.

Using (21)–(23) the geometrical coupling efficiency is computed numerically as a function of μ for various saturation parameters. The results are shown in Fig. 2. As it can be seen, the coupling becomes more efficient with increasing saturation as a consequence of transversal hole burning.

These results are directly applicable for the two limiting cases discussed in the preceding section. The threshold is given by (24) in both cases. If $\Delta\nu_h \ll \Delta\nu_{\text{av}}$, our treatment is expected to be a good approximation in the vicinity of threshold, where the signal linewidth $\Delta\nu_s$ is smaller than $\Delta\nu_h$. For pump powers well-above threshold spectral hole burning occurs, and significant enhancement of $\Delta\nu_s$ is anticipated. Thus, η_e increases more rapidly with S than predicted by (19). In the case $\Delta\nu_h \geq \Delta\nu_{\text{av}}$, $\Delta\nu_h$ has to be replaced by $\Delta\nu_{\text{ch}}$ in (13). Instead of hole burning, the flu-

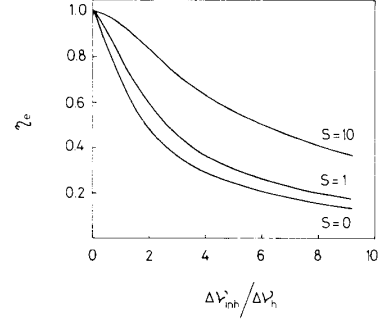


Fig. 1. Power extraction efficiency as a function of the ratio of inhomogeneous-to-homogeneous linewidth for different saturation parameters.

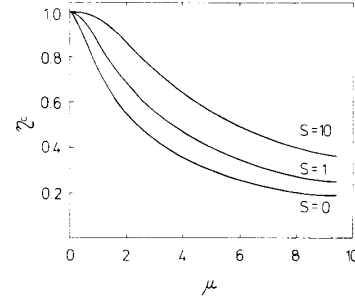


Fig. 2. Geometrical coupling efficiency as a function of $\mu = \overline{w_p^2}/\overline{w_l^2}$ for different values of the saturation parameter.

orescence profile is only flattened, if $\Delta\nu_{\text{ch}} \geq \Delta\nu_{\text{inh}}$. As a consequence, there is no drastic broadening of the laser emission spectrum expected as the pump power increases. Therefore, our model should be valid in the entire operating regime irrespective of pump levels. Obviously, this latter case implies a significantly higher η_e than the first one at low and moderate values of the saturation parameter because of $\Delta\nu_{\text{ch}} > \nu_n$. Thus, glass hosts with comparatively weak Stark splittings and large homogeneous linewidths allow more efficient CW laser operation than those with opposite properties.

The applicability of the above results for glass lasers with different active ions depends on the validity of approximations made in this section. Whereas most assumptions rest on direct knowledge of spectroscopic properties, some approximations may be justified by the ability of the model to predict experimental results.

It is clear from the above discussion that threshold can be drastically reduced by tight focusing of the pump beam and of the laser cavity mode in the gain medium. Furthermore, μ should be kept small for high-efficiency operation. However, thermal effects and their influence on the oscillating mode have to be also discussed before drawing conclusions concerning glass selection and cavity design.

IV. PERFORMANCE LIMITATIONS

Besides the two performance parameters P_{th} and η_{sl} discussed above there is a third important one: the highest

possible pump level at which (2) still holds, i.e., no performance limiting effects break in. This is especially important for mode locking requiring high gain for stable short-pulse generation.

The most severe performance limitations in a solid-state laser are of thermal nature. Heat dissipation in a solid laser material pumped by narrow-line radiation arises from the radiationless transitions in the material as a result of a quantum efficiency $\eta_q = h\nu_l/h\nu_p$ less than unity. Heating and cooling of the laser material result in a nonuniform transverse temperature distribution, which leads to a distortion of the laser beam due to a temperature and stress dependent variation of the refractive index, and due to bending of the end surfaces. These effects have two possibly severe consequences [3]: 1) thermal lensing (TL) and 2) thermal birefringence (TB).

To find an analytical solution of the heat conduction equation we assume the heat flow to be predominantly radial ($\partial T/\partial r \gg \partial T/\partial z$). In fact, this is a reasonable approximation if L and $1/\alpha$ are much greater than w_p , where α denotes the absorption coefficient at the pump wavelength. For a Gaussian radial distribution of the generated heat per unit volume the solution of the radial heat conduction equation [3] is found in form of power series

$$T(r, z) = T_0(z) - \frac{Q_0(z)}{4K} r^2 - \sum_{n=0}^{\infty} \frac{(-2)^n}{(n+1)!(n+1)} \left(\frac{r}{w_p}\right)^{2n} \quad (25)$$

where K stands for the thermal conductivity, $T_0(z)$ and $Q_0(z) = 2P_{in}(z)\alpha(1-\eta_q)/(\pi w_p^2)$ are the temperature and the heat dissipated per unit volume along the cavity axis, respectively. $P_{in}(z)$ denotes the pump power passing through the xy plane at the coordinate z in the gain medium. $T_0(z)$ is determined by boundary conditions.

The temperature rise causes a change in index due to the nonzero partial derivatives of the refractive index with respect to the temperature and mechanical stress. Latter arises from temperature gradients in a heated material. The variation of the refractive index in an isotropic medium due to thermal influence can be characterized by three material constants [25], [26]: $\partial n/\partial T$ the temperature coefficient at constant stress equal to zero, $B_{\parallel} = -\partial n/\partial \sigma_{\parallel}$ and $B_{\perp} = -\partial n/\partial \sigma_{\perp}$, the changes in index with respect to a change in stress directed parallel and perpendicular to the direction of polarization, respectively. The nonzero value of either of the three coefficients may lead to thermal lensing whereas a nonzero difference between B_{\perp} and B_{\parallel} causes birefringence.

The radial dependence of the index change due to the temperature coefficient $\partial n/\partial T$ can be directly obtained by multiplying with the temperature profile (25). To calculate the change in index due to the photoelastic effect is somewhat complicated. We assume L and $1/\alpha$ to be much greater than w_p now as before, which allows the assumption of a plain strain in the material. Owing to these simplifications the nondiagonal elements of the stress tensor

vanish in a cylindrical coordinate system whereas the diagonal elements are integral functions of the temperature $T(r, z)$ [25], [26]. These integrations can be carried out analytically for power functions and therefore also for the power series in (25). The principal axes of the index change coincide with those of the local cylindrical system resulting in different changes of index for radial and tangential components of the field.

Taking only the first term of the power series in (25) $T(r, z)$ leads to a quadratic index profile and thereby to the forming of an effective spherical lens [27]. The focal length of the thermal lens for the radial and tangential polarization components can be written

$$f_{r,\theta} = \frac{K\pi w_p^2}{P_{in}\eta_q(1-\eta_q)} \left(\frac{dn}{dT}\right)_{r,\theta}^{-1} \quad (26)$$

P_{in} is the incident pump power and $(dn/dT)_{r,\theta}$ is the effective temperature coefficient of the refractive index which is given by

$$\left(\frac{dn}{dT}\right)_{r,\theta} = \frac{\partial n}{\partial T} + \frac{2\beta E}{1-\kappa} B_{r,\theta} + \frac{4\beta w_p(n-1)}{L} \quad (27)$$

where the second term represents the stress dependent change of the index and the last term accounts for the end-face distortions [28]. β is the coefficient of thermal expansion, E stands for Young's modulus, and κ is the Poisson's ratio. The coefficients $B_{r,\theta}$ are defined by $B_r = (B_{\parallel} + 7B_{\perp})/8$ and $B_{\theta} = (3B_{\parallel} + 5B_{\perp})/8$, respectively. In practice $w_p/L \ll 1$, and the last term is negligible consequently $(dn/dT)_{r,\theta}$ can be regarded as a material parameter. As expected the strength of thermal lensing is proportional to (dn/dT) . Equation (26) applies for rays propagating close to the optical axis of the resonator while the thermal lens shows strong spherical aberration for $r > w_p/2$ originating from higher order terms of the power series in (25), and resulting in an increase of the focal length.

The birefringence can be characterized by polarization phase shift of the light emerging from the laser glass:

$$\frac{2\pi}{\lambda} \int_{z=0}^L |\Delta n_r - \Delta n_{\theta}| dz = \frac{P_{in}\eta_q(1-\eta_q)}{A_{TB}} \frac{r^2}{w_p^2} \left[1 - \epsilon \left(\frac{r^2}{w_p^2}\right) \right] \quad (28)$$

where

$$A_{TB} = \frac{2K\lambda_l(1-\kappa)}{\beta E |B_{\parallel} - B_{\perp}|} \quad (29)$$

ϵ is a monotonically increasing function of $(r/w_p)^2$ taking values between zero and one [29]. It results from higher order terms of the power series in (25) causing the birefringence to approach a finite value rather than infinity as $(r/w_p)^2 \rightarrow \infty$. Obviously, the expression of TB goes to zero if β , the coefficient of thermal expansion, vanishes, or if the coefficient of stress birefringence ($B_{\parallel} - B_{\perp}$) is zero. Both TL and TB are proportional to the quan-

tum defect $(1 - \eta_q)$ and inversely proportional to the heat conductivity of the glass host.

To answer the question at which pump levels the effects discussed above become critical, some information about the cavity is necessary. The requirement of a long cavity (needed for mode locking) and of a tight focusing (needed for low threshold) can be satisfied by a folded cavity [30].

TL effectively inserts an additional lens at the beam waist into the cavity, causing the optical resonator to become unstable as the focal length is approaching a critical value. In a conventional two-mirror resonator a lens inserted into the cavity gives rise to significant changes in the parameters of the oscillating mode if the focal length is comparable with the length of the resonator. A small spot folded cavity tolerates much shorter focal lengths perturbing the cavity than the resonator length, on the condition that the lens is placed at the waist of the cavity mode. This is a straightforward consequence of the fact that the propagation of a tightly-focused Gaussian beam is nearly unaffected by an additional lens at the beam waist as long as its focal length is significantly greater than the confocal parameter of the beam.

In fact, using the concepts of Kogelnik *et al.* [30] it can be shown that the resonator becomes unstable at $f_{\text{crit}} \approx S$ where $2S$ is the stability range of the unperturbed cavity, being approximately equal to the confocal parameter of the cavity mode (provided that the resonator is adjusted to the middle of the stability range). Combining these results with the expression of the thermal focal length a critical pump power leading to instability due to TL can be obtained:

$$P_{\text{crit}}^{\text{TL}} = \frac{A_{\text{TL}}}{\eta_a(1 - \eta_q)} \mu \quad (30)$$

where

$$A_{\text{TL}} = K |dn/dT|^{-1} \lambda_l \quad (31)$$

$|dn/dT|$ is the greater one of $|dn/dT|_{r,\theta}$ and λ_l denotes the laser wavelength. A_{TL} is a material parameter depending on mechanical, thermal, and optical properties of the host. Apparently, high quantum efficiency and increasing μ reduce the effect of TL. Fig. 3 shows $P_{\text{crit}}^{\text{TL}}$ versus μ for different values of the quantum efficiency.

TB also sets a limit to the pump power in a linearly polarized laser. The losses experienced by the circulating radiation due to the depolarization process increase with pump power. At a critical input power level the net gain stops increasing with pump power because the enhancement of the gain is compensated for by that of the depolarization loss. The determining equation for this critical input power is given by

$$\frac{\partial}{\partial P_{\text{in}}} \{ [1 + G_{\text{rs}}(P_{\text{in}}, P)] T_{\text{rs}}(P_{\text{in}}) \} = 0 \quad (32)$$

where $T_{\text{rs}}(P_{\text{in}})$ is a single-pass transmission factor less than unity owing to depolarization loss in the active ma-

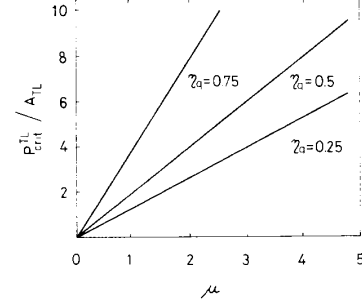


Fig. 3. Critical pump power due to thermal lensing normalized by the material parameter A_{TL} as a function of μ for different quantum efficiencies.

terial. Making use of (2) and (10), (32) becomes

$$\frac{\partial T_{\text{rs}}}{\partial P_{\text{in}}} = -\frac{\delta}{\delta + 2} \frac{T_{\text{rs}}}{P_{\text{in}}} \quad (33)$$

To obtain the expression of $T_{\text{rs}}(P_{\text{in}})$ we recapitulate a well-known formula giving the transmitted intensity when a birefringent crystal is placed between polarizer and analyzer that are parallel [31]:

$$\frac{I_{\text{out}}}{I_{\text{in}}} = 1 - \sin^2(2\phi) \sin^2(\Delta/2) \quad (34)$$

where ϕ is the angle between the polarizer and one of the principal birefringence axes and Δ is the polarization phase shift. Assuming both $r(x, y, z)$ and $s(x, y, z)$ to be fundamental Gaussian modes, from (34) can be derived

$$\begin{aligned} T_{\text{rs}}(P_{\text{in}}) &= T(\mu, P_{\text{in}}) \\ &= 4\mu \int_0^\infty e^{-2\mu u^2} \left[1 - \frac{1}{2} \sin^2 \frac{\Delta(u, P_{\text{in}})}{2} \right] u \, du \end{aligned} \quad (35)$$

where

$$\Delta(u, P_{\text{in}}) = \frac{P_{\text{in}} \eta_a (1 - \eta_q)}{A_{\text{TB}}} u^2 [1 - \epsilon(u^2)]. \quad (36)$$

In (35) and (36) u represents the normalized radial coordinate r/w_p . To solve (33) the integral in (35) and its partial derivative with respect to P_{in} have to be evaluated numerically. The solution of (33) yields $P_{\text{crit}}^{\text{TB}}$ depending on the cavity parameters δ and μ . $P_{\text{crit}}^{\text{TB}}$ is shown in Fig. 4 as a function of μ for different values of δ . It is a monotonically increasing function of μ , which follows from (28). Decreasing cavity losses results in a reduced $P_{\text{crit}}^{\text{TB}}$, a consequence of the fact that the polarization phase shift accumulates during several passes through the active material *during the cavity lifetime*. In contrast with the critical intensity for TL, $P_{\text{crit}}^{\text{TB}}$ does not go to zero as $\mu \rightarrow 0$.

Besides TL and TB there is a third thermal effect limiting the pump power: thermal damage (TD) of the laser material. TD occurs when the temperature along the cavity axis in the active medium reaches the softening point T_s of the host. Assuming a cylindrical symmetry of the heat sink contacted to the laser medium $T_0(z)$ can be writ-

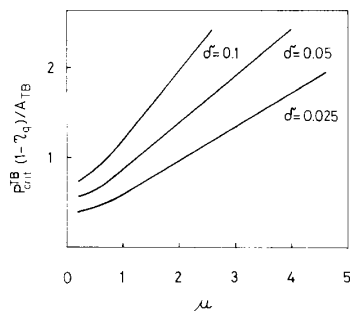


Fig. 4. Critical pump power due to thermal birefringence normalized by the material parameter A_{TB} as a function of μ for various cavity round-trip losses.

ten from (25) as

$$T_0(z) = T_{\text{amb}} + \frac{Q_0(z) w_p^2}{4K} \xi \quad (37)$$

where T_{amb} is the temperature of the heat sink and

$$\xi = \lim_{x \rightarrow \infty} \sum_{n=0}^{\infty} \frac{(-2)^n x^{2n+2}}{(n+1)!(n+1)} \quad (38)$$

provided that the heat sink is far away from the cavity axis compared to w_p . From (37) straightforward algebra yields:

$$P_{\text{crit}}^{\text{TD}} = \frac{A_{\text{TD}}}{\rho\alpha} \quad (39)$$

where ρ is the portion of the absorbed pump intensity which is converted into heat and A_{TD} is the scaling parameter for thermal damage:

$$A_{\text{TD}} = \frac{2\pi}{\xi} K(T_s - T_{\text{amb}}). \quad (40)$$

When the laser is oscillating $\rho \approx 1 - \eta_a$, but in the absence of stimulated emission ρ may deviate considerably from this value, depending on the fluorescence branching ratios for transitions from the metastable to the terminal levels. The greater of these two values should be substituted into (39).

Excessive heating might also lead to mechanical damage, when the tension at the edge of the plate or slab exceeds the tensile strength of the host material. The stresses depend not only on the temperature distribution but also on the geometrical sizes of the medium. Sufficiently-large transversal dimensions should prevent this type of damage from occurring.

The above considerations remain valid also for mode-locked operation. In the case of mode locking there appears an additional effect possibly limiting performance: self-focusing due to the index change $\Delta n = n_2 I$, where n_2 is the nonlinear index and I is the intensity of the laser pulse. The critical peak intensity of the circulating pulse is given by $P_{\text{crit}}^{\text{SF}} \approx \lambda_l^2 / (16\pi n_2)$. $P_{\text{crit}}^{\text{SF}}$ typically takes values in excess of 1 GW, which is a value never reached before thermal effects become critical. As a consequence,

TL, TB, and TD are the ultimate performance limiting effects both in CW and in CW mode-locked operation.

V. DESIGN CONSIDERATIONS

The performance of an end-pumped CW four-level glass laser is characterized by (20), (24), (29), (31), and (40). The spot sizes of the cavity mode and the pump beam appear explicitly only in the expressions of threshold and implicitly in that of critical pump power for thermal damage. The reduction of the signal and pump spot sizes lowers both P_{th} and $P_{\text{crit}}^{\text{TD}}$. Optimum performance can be achieved by appropriate choice of the parameters of the cavity and of the laser material, which depends on the pump power.

Let us first consider the case of low-power operation when thermal damage may be excluded. Under these circumstances the reduction of the signal spot size lowers the threshold without any compromise. In a bulk laser material of length L the minimum value of w_l^2 is proportional to L , which is inversely proportional to the dopant concentration (at a fixed η_a). However, high concentration reduces τ as a result of ion-ion interactions [32]. To find a scaling of minimum threshold with the spectroscopic properties of the dopants and host parameters, Fan and Byer [33] introduced figures of merit for the threshold of end-pumped solid-state lasers. On the basis of their concepts and using the above considerations the figure of merit M_{th} for minimum threshold of end-pumped four-level glass lasers in the low-power regime is given by

$$M_{\text{th}} = \sigma\tau_0\eta_p N_{1/2}\sigma_a \quad (41)$$

where τ_0 is the zero concentration lifetime, $N_{1/2}$ is the concentration halving τ_0 , and σ_a stands for the absorption cross section at the pump wavelength. We assumed that the bulk losses such as scattering or impurity absorption are much smaller than the total round-trip loss of the resonator. Equation (41) also holds for a quasi-three-level laser as long as the loss resulting from parasitic absorption by lower laser level population is considerably smaller than other losses in the cavity.

A figure of merit for the slope efficiency is defined as

$$M_{\text{se}} = \eta_q\eta_p\eta_{e0} \quad (42)$$

where $\eta_{e0} = \eta_e(S=0)$. Both η_q and η_p depend on the position of the energy levels involved in the excitation and deexcitation processes. A small difference between pump and signal photon energies implies not only high quantum efficiency but also high η_p due to fast multiphonon relaxation between levels with small energy difference [32]. η_{e0} is influenced by $\Delta\nu_{\text{av}}$, $\Delta\nu_h$, and $\Delta\nu_{\text{inh}}$, as discussed in Section III.

Whereas M_{se} varies in different hosts mainly due to the variation of $\Delta\nu_h/\Delta\nu_{\text{av}}$ the parameters M_{th} , A_{TL} , A_{TB} , and A_{TD} comprise many constants depending on the host. In Table I numerical values of these parameters are given for different glasses. M_{th} is calculated for the ${}^4F_{3/2}$ - ${}^4I_{11/2}$

TABLE I
FIGURES OF MERIT OF DIFFERENT LASER GLASSES. DATA ARE TAKEN FROM THE SCHOTT CATALOG OF LASER GLASSES FOR THE SILICATE GLASS LG 680 AND THE PHOSPHATE GLASS LG 760

Glass Host	M_{th} $10^{-23} \text{ cm} \times \text{s}$	A_{TL} W	A_{TB} W	A_{TD} W/mm
Silicate	7.9	0.19	1.28	1.3
Phosphate	30.5	0.54	0.80	0.45

transition ($1.06 \mu\text{m}$) in Nd, while the thermal parameters are only host-dependent. The phosphate glass has much higher M_{th} than the silicate glass owing to its higher stimulated emission cross section and weaker concentration quenching. Therefore, it is more suitable for low-power operation than a silicate glass. The A coefficients become relevant at high pumping levels. Whereas the relatively low P_{crit}^{TD} of the phosphate glass can be increased at the cost of enhanced threshold, the increase of the low P_{crit}^{TL} of the silicate glass can only be realized by reducing the slope efficiency. Consequently, phosphate glass appears to be the better host in a CW end-pumped glass laser both for low and for high pump powers.

After selecting an appropriate host the main aspects of the design can be summarized as follows. For minimum threshold the dopant concentration should maximize the product $N\tau(N)$. The doping level determines the length L of the active medium by the requirement of a high η_a . From the active length the minimum average signal spot size in the laser medium is calculated. For this minimum signal spot the pump parameter μ may take values in the region $\mu \geq \eta_q$ [34]. Efficient operation requires $\mu \leq 1$. For high pumping levels, however, the choice of somewhat higher μ may be expedient thereby considerably increasing the critical pump powers P_{crit}^{TL} , P_{crit}^{TB} at the expense of a tolerable reduction of the slope efficiency.

Nevertheless, to avoid the onset of TEM_{01} mode oscillation μ should be kept smaller than δ_{01}/δ_{00} where δ_{01} and $\delta_{00} = \delta$ are the round-trip losses for the TEM_{01} and TEM_{00} modes, respectively [35]. μ and $\overline{w_i^2}$ give the value of w_p^2 which allows P_{crit}^{TD} to be calculated. In case the laser is to be pumped at comparable or higher levels than P_{crit}^{TD} , the dopant concentration should be reduced according to (39). Whereas P_{crit}^{TD} increases with N^{-1} , P_{th} goes up more slowly because of $\tau = \tau(N)$. The desirable spot size may be realized by appropriate choice of the radius of the focusing mirror for a given cavity length [30]. Finally, the output power is maximized by optimum output coupling, which is also a means for increasing P_{crit}^{TB} if necessary.

Let us follow the design procedure on the example of Nd:phosphate glass LG 760. The product $N\tau(N)$ takes its maximum value for $N \approx 8$ percent (weight percent). For this concentration $\alpha = 18 \text{ cm}^{-1}$ and $L = 1.2 \text{ mm}$ yield $\eta_a \approx 0.9$ at $\lambda_p = 0.8 \mu\text{m}$. The minimum average signal spot size is $(\overline{w_i^2})^{1/2} \approx 20 \mu\text{m}$ assuming a plate of thickness $t = 1 \text{ mm}$ to be inserted at Brewster's angle into the cavity. To find a suitable value for the pump param-

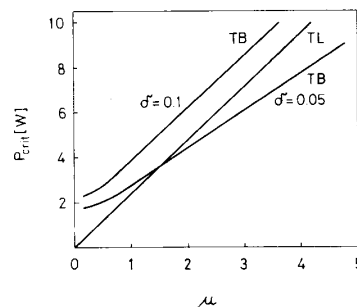


Fig. 5. Critical pump powers as a function of μ for phosphate glass LG 760.

eter we should cast a glance at Fig. 5 where the critical pump powers as a function of μ are shown. For this high value of N the limiting effect is TD, and μ should be chosen as small as possible, i.e., $\mu = 0.75$. Strong pumping requires a correspondingly-reduced dopant concentration and possibly a somewhat increased μ .

In case the pump beam is not diffraction limited, the signal and pump spot sizes change their roles in the design procedure. For a given L the minimum w_p^2 is to be determined and then μ can be controlled with the signal spot size. Generally, a nondiffraction-limited pump beam implies always a higher threshold than a diffraction-limited one.

VI. EXPERIMENTS

A Nd:glass laser suitable for continuous wave mode locking was built taking into account design aspects discussed above. The laser emits radiation at $\lambda_1 = 1.054 \mu\text{m}$. The gain material is a 1 mm thick phosphate glass (LG 760) plate with 8 weight percent Nd^{3+} concentration. The transversal dimensions are $10 \times 10 \text{ mm}$. The plate between two copper plates is inserted at Brewster's angle at the TEM_{00} mode waist into a folded resonator compensated against astigmatism [30], as shown in Fig. 6. Our approach of folding the resonator two times reduces the sizes of the system and enables us to couple the pump beam into the oscillator through the folding mirror $M2$ (the reflection loss of $M2$ is ≈ 3 percent).

This method has two significant advantages over that of coupling the pump radiation through $M4$ into the cavity: 1) it easily allows collinear alignment of resonator and cavity beams and 2) mirror $M4$ may also be highly reflecting for both pump and signal wavelengths thereby allowing the pump beam to propagate twice through the laser medium. This makes possible the reduction of the length L of the active medium by a factor of two allowing the reduction of threshold by the same factor. This approach is especially important in a quasi-three-level laser, in which further lowering of threshold is expected owing to reduced parasitic absorption.

Therefore, achieving oscillation at $\lambda = 0.93 \mu\text{m}$ in Nd:glass seems to be possible with tolerable threshold.

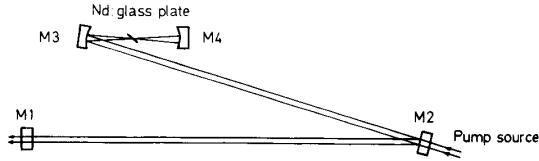


Fig. 6. Schematic of the CW Nd:glass laser oscillator. $M1$ is a plane mirror with a reflectance of 97.5 percent. $M2$ is a dichroic plano mirror with high reflectance at $1.054 \mu\text{m}$ and low reflectance (< 3 percent) at $0.8 \mu\text{m}$. $M3$ and $M4$ are concave mirrors with $R_3 = 2R_4 = 10 \text{ cm}$ supplied with HR coating for both wavelengths.

In our case, absorption efficiency of nearly one is attained in this way at $\lambda = 799 \text{ nm}$ in a gain material as short as $L = 1.2 \text{ mm}$. Unfortunately, this scheme does not work well with a diode laser as the pump source. The diode laser beam should be coupled into the cavity preferably through mirror $M4$, the radius of which may be chosen sufficiently small without influencing cavity design to allow tight focusing of the diode beam.

The confocal parameter b of the TEM_{00} mode is matched the gain length by suitable choice of cavity parameters: $R_3 = 2R_4 = 5 \text{ cm}$ and a cavity length of 180 cm yield a confocal parameter $b = 1.4 \text{ mm}$ for the fundamental mode of the empty cavity. As a result, a nearly minimum average spot size of $(w_l^2)^{1/2} \approx 20 \mu\text{m}$ is achieved in the active medium. The 799 nm line of a krypton laser is used as a pump source in our experiments simulating well diode laser pumping. The average spot size of the pump beam is $(w_p^2)^{1/2} \approx 18 \mu\text{m}$ yielding $\mu = 0.8$.

By comparing the thresholds for different output couplings the internal cavity round-trip loss is measured to be 1.9 percent. Thus, the total round-trip loss is $\delta = 4.4$ percent for an output coupling $T = 2.5$ percent. Substituting these values with the data $\sigma = 4.2 \times 10^{-20} \text{ cm}^2$ and $\tau = 220 \mu\text{s}$ [36] and $\eta_a = \eta_p = 1$, (24) predicts $P_{\text{th}} = 8.2 \text{ mW}$. The measured output power as a function of the input power is shown in Fig. 7. The threshold pump power measured is $P_{\text{th}} = 10.5 \text{ mW}$. The discrepancy between the theoretically-predicted value and the experimental result can be attributed to a small residual misalignment of the cavity and/or of the pump beam.

The slope efficiency containing the factors η_e and η_c depends on the circulating signal power and can be written as $\eta_{\text{sl}}(S) = \eta_{\text{sl},\infty} \eta_e(S) \eta_c(S)$, where $\eta_{\text{sl},\infty} = (T/\delta) \eta_a \eta_p = 43$ percent is the slope efficiency for infinite pump power. Taking the value of the effective linewidth $\Delta\nu = 176 \text{ cm}^{-1}$ [36] for the $1.054 \mu\text{m}$ transition in the potassium-barium-phosphate glass LG 760 the average distance between adjacent Stark frequencies is estimated to be $\Delta\nu_{\text{av}} \approx 30 \text{ cm}^{-1}$ [9]. Approximate values of $\Delta\nu_h$ and $\Delta\nu_{\text{inh}}$ are obtained from [14] to be $\Delta\nu_h \approx 45 \text{ cm}^{-1}$ and $\Delta\nu_{\text{inh}} \approx 80 \text{ cm}^{-1}$.

These numbers suggest that the limiting case $\Delta\nu_h \geq \Delta\nu_{\text{av}}$ should apply to our laser glass. Using the above values of $\Delta\nu$ and $\Delta\nu_{\text{inh}}$, the deconvolution of the Voigt function yields $\Delta\nu_{\text{ch}} \approx 135 \text{ cm}^{-1}$. The theoretically predicted $\eta_{\text{sl}}(S)$ is plotted in Fig. 8 (upper curve). The dots with

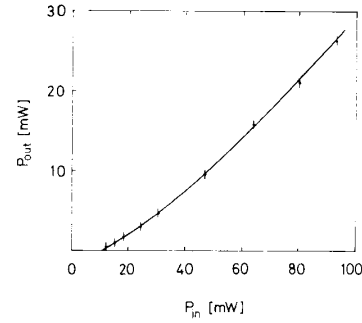


Fig. 7. Output power as a function of the incident pump power upon the gain material. The laser is pumped at 799 nm . The output coupler has a transmission of $T = 2.5$ percent.

error bars represent the experimental results. For comparison, the lower curve shows the prediction of our model in a region $S < 1$ if $\Delta\nu_h \ll \Delta\nu_{\text{av}}$. Although neither of the two curves fits to the experimental points, a difference between experimental results and the upper curve can be explained with the same arguments as in the case of P_{th} .

In the ratio of $\eta_{\text{sl}}(S \approx 10)/\eta_{\text{sl}}(S \approx 0)$ the effects of cavity or pump beam misalignments cancel allowing a meaningful comparison with theory. As a matter of fact, the measured value of this ratio is 1.50, in excellent agreement with the prediction of 1.46 for the case $\Delta\nu_h \geq \Delta\nu_{\text{av}}$, while in the case $\Delta\nu_h \ll \Delta\nu_{\text{av}}$ this ratio is expected to be between 2 and 3. In accordance with these findings, the spectrum of the laser output does not broaden considerably with increasing saturation. Consequently, the homogeneously-broadened Stark transitions should overlap to a great extent in the phosphate laser glass LG 760. As a result, η_e is high also at low pump levels and the output spectrum remains narrow also at high pump levels.

To find some experimental evidence for the theoretical considerations on thermal effects the laser is pumped by the 752 nm line of the krypton laser, which is much stronger than that at 799 nm . The output of the laser is split into two beams with a Glan polarizer allowing the measurement of the depolarization of the laser output. The theory presented in the preceding section yields the following expression for the depolarization ratio:

$$D = \frac{P_{\text{out}}^{\perp}}{P_{\text{out}}^{\parallel}} = D_0 + \frac{2[1 - T(\mu, P_{\text{in}})]}{\delta_{\perp}} \quad (43)$$

where the symbols \perp and \parallel represent polarization directions perpendicular and parallel to the main polarization direction of the laser. Correspondingly, δ_{\perp} denotes the round-trip loss for the perpendicular polarization. D_0 is the small-signal depolarization which is measured to be 5×10^{-3} in our laser. Fig. 9 shows measured values of D for two different values of the pump parameter. The curves are power dependences predicted from (43). $\mu = 0.4$ is realized by shortening the resonator length by a factor of two. Considering the fact that there are no fit parameters in (43) the theoretical predictions compare fairly well with the measured data.

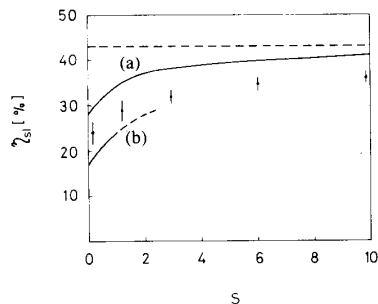


Fig. 8. Slope efficiency versus saturation parameters. (a) $\Delta\nu_h \geq \Delta\nu_{av}$, (b) $\Delta\nu_h \ll \Delta\nu_{av}$, with $\Delta\nu_h = 45 \text{ cm}^{-1}$, $\Delta\nu_{eh} = 135 \text{ cm}^{-1}$, and $\Delta\nu_{inh} = 80 \text{ cm}^{-1}$. The dashed line is $\eta_{sl,\infty}$ and the dots are experimental results.

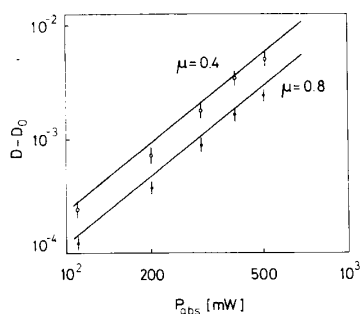


Fig. 9. Depolarization ratios measured for two different values of the pump parameter μ . The curves are predictions from (43).

It is worth mentioning that the transversal mode stability is very poor for a μ as small as 0.4. A small misalignment of the cavity or of the pump beam gives rise to higher order mode oscillation up to the TEM_{03} mode. However, even for this low value of μ the Gaussian profile of the output beam appears to be nearly unaffected for pumping levels below $P_{\text{crit}}^{\text{TD}}$, as expected from Fig. 5.

When the laser oscillates $P_{\text{crit}}^{\text{TD}}$ is measured to be $\approx 1 \text{ W}$. Substituting $\alpha = 11 \text{ cm}^{-1}$ and $\rho = 0.29$ into (39) we obtain $P_{\text{crit}}^{\text{TD}} = 1.4 \text{ W}$. One reason for the discrepancy may be the presence of residual scratches, defects, and imperfections on the surface. At these points the electric field in the pump beam is significantly intensified facilitating the start of the damage process. Surface contaminations also significantly reduce $P_{\text{crit}}^{\text{TD}}$. Therefore, care has to be taken to keep the glass plate as clean as possible. Moving the active medium away from the focal point of the folding mirror, no noticeable change in $P_{\text{crit}}^{\text{TD}}$ is observed, i.e., the pump beam diameter does not influence thermal damage as predicted by the theory.

Preventing oscillation we observe a significantly reduced $P_{\text{crit}}^{\text{TD}}$, which is compatible with $\rho = 0.38$. Surprisingly, the fluorescence branching ratios for transitions from the upper laser level to the terminal levels [32] yield a value $\rho = 0.25$. The discrepancy points to multiphonon relaxation from the metastable (${}^4F_{3/2}$) to the upper (${}^4I_{15/2}$) terminal level. Assuming this effect to be mainly responsible for the increased ρ we obtain the multiphonon decay rate $W_{\text{mp}} \approx 700 \text{ s}^{-1}$.

Finally, it should be noted that the high temperature gradient $\partial T/\partial r \approx 10^3 \text{ K/mm}$ present in the laser material when pumped by hundreds of milliwatts result in high stresses if the transversal sizes of the plate are small. When the distance between the active region and one of the edges is reduced to $\approx 2 \text{ mm}$, the glass is ruptured.

VII. SUMMARY

We have modeled the operation of end-pumped four-level CW glass lasers discussing two limiting cases where the homogeneous linewidth is comparable to or much smaller than the average spacing between adjacent Stark frequencies within the laser transition. We have considered thermal effects such as thermal lensing, birefringence, and damage which may severely affect laser performance at high pump powers. Our discussion shows that thermal effects such as lensing and birefringence in end-pumped solid-state lasers depend neither on the cavity mode volume nor on the pump beam volume in the gain material, but only on their ratio. Therefore, to achieve efficient operation small-spot cavity design should be preferred taking into account the damage threshold of the material.

Figures of merits (M_{th} , M_{se} , A_{TL} , A_{TB} , and A_{TD}) have been introduced scaling the performance parameters such as threshold, slope efficiency, and critical pump powers. These figures of merits allow easy comparison of the performance of any four-level glass laser with that of Nd:glass laser, for which experimental results are presented in this paper. Finally, we have demonstrated that low-threshold, high-efficiency operation is possible in a long-cavity Nd:phosphate glass laser pumped longitudinally at $\lambda = 0.8 \mu\text{m}$, and critical pump powers can be increased up to a few watts retaining the high efficiency achieved in low-power operation. The recent availability of high-power GaAlAs diode lasers emitting at $0.8 \mu\text{m}$ will make possible the building of a highly efficient, compact, all-solid-state laser system generating stable picosecond (or subpicosecond) pulses with high energy.

ACKNOWLEDGMENT

The authors gratefully thank H. J. Jung and the Schott Glaswerke, Mainz, for providing the laser material. They are also indebted to T. Brabec for valuable suggestions.

REFERENCES

- [1] A. J. DeMaria, W. H. Glenn, M. J. Brienza, and M. E. Mach, "Picosecond laser pulses," *Proc. IEEE*, vol. 57, pp. 2-25, 1969.
- [2] M. A. Duguay, J. W. Hansen, and S. L. Shapiro, "Study of the Nd:glass laser radiation," *IEEE J. Quantum Electron.*, vol. QE-6, pp. 725-743, 1970.
- [3] W. Koechner, *Solid State Laser Engineering*. New York: Springer-Verlag, 1976.
- [4] S. Kishida, K. Washio, S. Yoshikawa, and Y. Kato, "CW oscillation in a Nd:phosphate glass laser," *Appl. Phys. Lett.*, vol. 34, pp. 273-275, 1979.
- [5] S. Basu and R. L. Byer, "Continuous-wave mode-locked Nd:glass laser pumped by a laser diode," *Opt. Lett.*, vol. 13, pp. 458-460, 1988.
- [6] S. A. Stobel, P. T. Ho, C. H. Lee, and G. L. Burdge, "Continuous-wave mode-locked neodymium:phosphate glass laser," *Appl. Phys. Lett.*, vol. 45, pp. 1171-1172, 1984.

- [7] L. Yan, J. D. Ling, P. T. Ho, and C. H. Lee, "Picosecond-pulse generation from a continuous-wave neodymium:phosphate glass laser," *Opt. Lett.*, vol. 11, pp. 502-503, 1986.
- [8] M. J. Weber, "Laser excited fluorescence spectroscopy of glass," in *Laser Spectroscopy of Solids*, W. M. Yen and P. M. Selzer, Eds. W. Germany: Berlin Springer-Verlag, 1981, pp. 189-239.
- [9] D. W. Hall, R. A. Haas, W. F. Krupke, and M. J. Weber, "Spectral and polarization hole burning in neodymium glass lasers," *IEEE J. Quantum Electron.*, vol. QE-19, pp. 1704-1717, 1983.
- [10] M. M. Mann and F. L. DeShazer, "Energy levels and spectral broadening of neodymium ions in laser glass," *J. Appl. Phys.*, vol. 41, pp. 2951-2957, 1970.
- [11] V. I. Nikitin, M. S. Soskin, and A. I. Khizhnyak, "Uncorrelated inhomogeneous broadening as the cause for the narrow-band output of an Nd³⁺-activated phosphate glass laser," *Sov. Tech. Phys. Lett.*, vol. 3, pp. 5-6, 1977.
- [12] C. Brecher, L. A. Riseberg, and M. J. Weber, "Line-narrowed fluorescence spectra and site-dependent transition probabilities of Nd³⁺ in oxide and fluoride glasses," *Phys. Rev. B*, vol. 18, pp. 5799-5811, 1978.
- [13] V. I. Nikitin, M. S. Soskin, and A. I. Khizhnyak, "Influence of uncorrelated inhomogeneous broadening of the 1.06 μ band of the Nd³⁺ ions on laser properties of neodymium glasses," *Sov. J. Quantum Electron.*, vol. 8, pp. 788-790, 1978.
- [14] J. M. Pellegrino, W. M. Yen, and M. J. Weber, "Composition dependence of Nd³⁺ homogeneous linewidths in glasses," *J. Appl. Phys.*, vol. 51, pp. 6332-6336, 1981.
- [15] D. W. Hall and M. J. Weber, "Polarized fluorescence line narrowing measurements of Nd laser glasses: Evidence of stimulated emission cross section anisotropy," *Appl. Phys. Lett.*, vol. 42, pp. 157-159, 1983.
- [16] K. Kubodera and K. Otsuka, "Single-transverse-mode LiNdP₄O₁₂ slab waveguide laser," *J. Appl. Phys.*, vol. 50, pp. 653-659, 1979.
- [17] D. G. Hall, R. J. Smith, and R. R. Rice, "Pump-size effects in Nd:YAG lasers," *Appl. Opt.*, vol. 19, pp. 3041-3043, 1980.
- [18] M. J. F. Digonnet and C. J. Gaeta, "Theoretical analysis of optical fiber laser amplifiers and oscillators," *Appl. Opt.*, vol. 24, pp. 333-342, 1985.
- [19] T. Y. Fan and R. L. Byer, "Modeling and CW operation of a quasi-three-level 946 nm Nd:YAG laser," *IEEE J. Quantum Electron.*, vol. QE-23, pp. 605-612, 1982.
- [20] A. Y. Cabezas and R. P. Treat, "Effect of spectral hole-burning and cross relaxation of the gain saturation of laser amplifiers," *J. Appl. Phys.*, vol. 37, pp. 3556-3563, 1966.
- [21] D. W. Hall, M. J. Weber, and R. T. Brundage, "Fluorescence line narrowing in neodymium laser glasses," *J. Appl. Phys.*, vol. 55, pp. 2642-2647, 1984.
- [22] J. T. Davies and J. M. Vaughan, "A new tabulation of the Voigt profile," *Astrophys. J.*, vol. 137, pp. 1302-1305, 1963.
- [23] A. Yariv, *Quantum Electronics*, 2nd ed. New York: Wiley, 1975.
- [24] The treatment of the general case $w_{ix} \neq w_{iy}$ allows to consider a Brewster-alignment of the active material. However, our results are only valid, if the pump beam just as the astigmatically compensated cavity mode is circular outside the active medium, i.e., $w_{px}/w_{py} = w_{iz}/w_{ix}$.
- [25] F. W. Quelle, "Thermal distortion of diffraction-limited optical elements," *Appl. Opt.*, vol. 5, pp. 633-637, 1966.
- [26] E. P. Riedel and G. D. Baldwin, "Theory of dynamic optical distortion in isotropic laser materials," *J. Appl. Phys.*, vol. 38, pp. 2720-2725, 1967.
- [27] W. Koehner, "Thermal lensing in a Nd:YAG laser rod," *Appl. Opt.*, vol. 9, pp. 2548-2553, 1970.
- [28] E. Snitzer and C. G. Young, in *Lasers*, vol. 2, A. K. Levine, Ed. New York: M. Dekker, 1968.
- [29] ϵ is given in form of a power series:
- $$\epsilon = -2 \sum_{n=1}^{\infty} \frac{(-2)^n}{(n+2)!} \left(\frac{r}{w_p}\right)^{2n}$$
- [30] H. W. Kogelnik, E. P. Ippen, A. Dienes and C. V. Shank, "Astigmatically compensated cavities for CW dye lasers," *IEEE J. Quantum Electron.*, vol. QE-8, pp. 373-379, 1972.
- [31] M. Born and E. Wolf, *Principles of Optics*. London, England: 1965.
- [32] D. C. Brown, *High-Peak-Power Nd: Glass Laser Systems*. Berlin, W. Germany: Springer-Verlag, 1981.
- [33] T. Y. Fan and R. L. Byer, "Diode laser-pumped solid-state lasers," *IEEE J. Quantum Electron.*, vol. 24, pp. 895-912, 1988.
- [34] This applies only to diffraction limited pump beams. Otherwise, e.g., when a diode laser is used as a pump source, the lower limit of μ may

be well above unity. In this case the minimum w_p^2 achievable should be found first and then w_i^2 is to be chosen to attain the desired pump parameter μ .

- [35] M. J. F. Digonnet and C. J. Gaeta, "Theoretical analysis of optical fiber laser amplifiers and oscillators," *Appl. Opt.*, vol. 24, pp. 333-342, 1985.

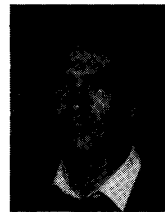
[36] Schott data sheet.



Ferenc Krausz was born in Mor, Hungary, in 1962. He received the B.Sc. degree from the Technical University of Budapest in 1985.

In 1987 he joined the Technische Universität Wien, Austria. He is a member of the staff with the Abteilung Quantenelektronik und Lasertechnik, pursuing the Ph.D. degree with research involving nonlinear optical investigations of organic semiconductors. His current research interests include diode laser pumping of solid-state lasers, the generation of ultrashort pulses, and

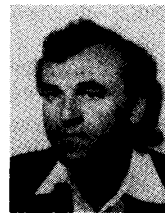
their application in nonlinear optics.



E. Wintner was born in St. Pölten, Austria, on March 9, 1950. He received the Ph.D. degree in physics from the Universität Wien, Austria, in 1976. His Ph.D. dissertation research concerned high-resolution electron microscopy of dislocations in metal single crystals.

Since 1976 he has been with the Technische Universität Wien, Austria, working in the field of nonlinear optics. From 1982 to 1984 he was a visiting scientist with E. P. Ippen at the Massachusetts Institute of Technology under a Max Kade

fellowship. In 1985 he became a permanent member of the staff as a dozent with the Abteilung Quantenelektronik und Lasertechnik, Technische Universität Wien. His research interests include the generation of ultrashort light pulses and their application to the study of ultrafast phenomena in optical materials.



Arnold J. Schmidt was born on August 7, 1938, in Vienna, Austria. He received the Ph.D. degree in physics from the Universität Wien in 1962.

After spending two years at the Ludwig Boltzmann Institut für Festkörperphysik, Wien, he joined the Department of Physics of the University of York, York, England, in 1966 as a Research Fellow. From 1971 until 1975 he was a Research Associate with the Department of Physics, University of California, Berkeley. Since 1975 he has been with the Technische Universität Wien, first as an Assistant Professor, from 1979 until 1986 as an Associate Professor and since 1986 as a Full Professor. His research interests center on nonlinear optics. He has worked on SHG in semiconductors and on ultrashort pulses. Recently, he studied SHG gratings on surfaces and in waveguides.

Dr. Schmidt is member of the American Physical Society, the Optical Society of America, and a number of other scientific societies.



Andrew Dienes was born in Hungary on October 22, 1939. He received the Ph.D. degree in physics from the California Institute of Technology, Pasadena, in 1967.

From 1967 to 1973 he was a Member of the Technical Staff at Bell Laboratories, Holmdel, NJ. During 1973-1974 he was a Visiting Mackay Professor with the Department of Electrical Engineering, University of California, Berkeley. In 1974 he joined the Department of Electrical Engineering, University of California, Davis, where

he has been a Full Professor since 1976. He also holds an Adjunct Professorship with the Department of Electrical Engineering, University of California, Berkeley. He has spent sabbatical visits at numerous institutions including the University of Brodeaux, France, the Weizmann Institute, Israel, and most recently, the Technical University of Vienna, Austria. His research interests center on ultrashort pulses and nonlinear optics but he has also been involved in solid-state and semiconductor lasers.